

# Model Based Force Control of Pneumatic Actuators with Long Transmission Lines

Melih Turkseven, Jun Ueda, *Member, IEEE,*

**Abstract**—Pneumatic systems with long transmission lines have recently gained popularity in tele-operated robotic applications, such as medical robots designed for operations in magnetic resonance (MR) rooms, mobile transportation robots, or pneumatically actuated humanoids. These tele-operated systems typically suffer from time delay and mass flow attenuation between the actuator and the drivers. The conventional paradigm in pneumatic system control is to employ standardized pneumatic system models that present large errors in characterizing the pressure dynamics of tele-operated actuators. The use of more accurate modeling approaches has been limited to flow simulations for their complexity. This study introduces a methodology that adapts an accurate non-linear line model to non-linear controllers. The proposed method utilizes the line model to formulate a virtual input that brings the system to the desired state. The contribution of the proposed method in the force control accuracy was experimentally validated for systems that involve 5 to 10 meter long transmission lines. The introduced method achieved up to 75% reduction in the error compared to a standard sliding-mode based force control at reference frequencies between 0.5 Hz to 2 Hz.

**Index Terms**—Force Control, Pressure Estimation, Transmission Lines, Tele-Operated Systems.

## I. INTRODUCTION

In the last two decades, pneumatically driven actuator systems have been widely used in the field of robotics for their mechanical advantages. Pneumatic actuation has a higher power density than conventional electric-motors [14], and provides a clean operation with low maintenance costs. Lately, the application areas of pneumatic actuation has expanded to tele-operation, in order to utilize some of its inherent practical advantages. The fact that air is inert to strong magnetic fields has been exploited in magnetic-resonance-imaging (MRI) compatible robots [2], [11]. MRI-compatible systems with pneumatic actuation typically require long transmission lines (5-7 meters) to keep the magnetic system components away from the imaging area. Pneumatic system components can be located apart in order to obtain a desired weight distribution in humanoid robot designs [23]. Tele-operation via long tubes has also been practiced for transportation systems where a mobile robot is designed to operate in challenging environments, being powered from a distance [13]. Pneumatic actuation has been shown to be very effective in these tele-operation applications; however, the presence of long transmission lines

M. Turkseven is with the School of Mechanical Engineering, Georgia Institute of Technology, Atlanta, GA, 30332 USA e-mail: mturkseven3@gatech.edu

J. Ueda is with the School of Mechanical Engineering, Georgia Institute of Technology, Atlanta, GA, 30332 USA e-mail: jun.ueda@gatech.edu

This research is funded by the National Science Foundation Center for Compact and Efficient Fluid Power (CCEFP).

limits the performance of those devices to low-bandwidth operations.

Pneumatic transmission lines, especially if the length to diameter ratio is high, have a significant influence on the pressure dynamics of a pneumatically operated system. Compressibility of the flowing media and finite velocity of pressure propagation cause an attenuation and a pure time delay in the mass flow. Also, a pressure gradient emerges along the lines due to the tube friction. As a result, the dynamic difference between the pressures at the terminals of a long connecting tube requires either an additional pressure sensor at the end of the line or an estimation method that characterizes the line dynamics. Given the complexity of compressible flow dynamics, pneumatic line models have been neglected in the field of robotics for simplicity and faster computation. A fairly standardized method characterizes the line as a dead volume and simply combines it to the actuator [6]. This generic approach provides a stable model for non-linear controllers, yet it cannot reflect the pressure inhomogeneity through the lines [25]. Even when accurate actuator pressure information is available, the standard pneumatic chamber model lacks accuracy on tele-operated systems above 0.5 Hz [24]. At a higher frequency, relatively more advanced methods are required to achieve a good accuracy in both the actuator pressure estimation and the mass flow rate through the lines.

The simplicity of standard modeling can be traded with high accuracy by the use of finite-element models. In general, the ultimate accuracy can be achieved by industrial simulation packages that involve heat transfer calculations and frequency-dependant friction in addition to fluid compressibility. However, such methodologies are computationally too expensive for real-time control applications [10] and often require equipment specific parameters [27]. Simpler methods based on averaging flow parameters within a finite number of volume partitions were introduced for faster computation [1], [27], [26]. Krichel and Sawodny adapted several hydraulic line modeling techniques to pneumatic systems, and suggested a time domain model to capture the transient behavior of pressure and flow rate through the tubes [10]. They divided the line into iso-thermal, spatial segments and established a discrete formulation of the governing equations. Despite its potential in real-time control, their approach has never been embedded to model based controllers.

Efficacy of a given model is contingent on its compatibility to well-established control methods. Yang et al. approximated the pressure dynamics of pneumatic tubes using a low-order transfer function with empirically obtained parameters [28], yet they didn't consider the line dynamics on their non-linear controller design. Li et al. discretized the line and obtained

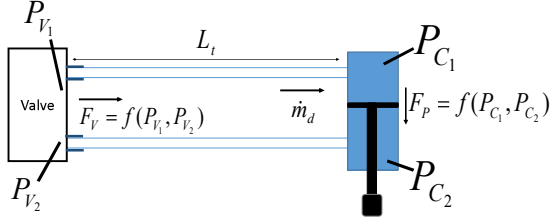


Fig. 1: The key elements of the proposed method of force control using a tele-operated pneumatic actuator

a time-domain model by adding heat transfer effects as well [12]. They demonstrated the use of their model in open-loop position control, and compared its performance against closed-loop control with valve pressure feedback. Hurmuzlu et al. obtained an explicit formula for the mass flow rate at the end of the line and implemented it in a sliding mode based controller. The controller was shown to be effective for line lengths up to 2 meters [15], [16]. Besides the limited range of transmission line length compared to those in the aforementioned applications, their model required measuring the actuator pressures. Their study illustrated the benefits of more accurate system modeling; yet, more comprehensive modeling methods were needed for systems with longer transmission lines.

## II. PROBLEM STATEMENT

Recent trends in the use of tele-operated pneumatically driven systems for human-robot interaction necessitate advanced approaches that account for compressible flow dynamics through long pneumatic tubing. Pneumatic line dynamics has been neglected in the control of robotic systems for low-bandwidth operations, such as needle insertion devices for minimally invasive surgeries [5], [4]. Conventional methods for characterizing the lines, e.g. assuming the line as a dead volume or linearizing the flow equations, have been satisfactory for low-frequency position control ( $\leq 1$  Hz) of tele-operated systems [28], [3]. However, the accuracy of those standard approaches diminishes at higher frequencies [25]. Therefore, control algorithms with more accurate modeling tools are needed for relatively faster operations such as haptic interfaces, rehabilitation robots and exoskeletons, in which force or impedance control is objected.

Long transmission lines have been characterized by a number of complex methods, yet only a few of them are suitable for online control applications. Detailed numerical simulation models are too complicated to be implemented in non-linear controllers and they often involve hardware specific parameters that limit the use of such methods [26], [12]. Krichel et al. presented an average friction model on a segmented profile that is feasible for online control applications [10]. Their study suggested the use of numerical time-domain models instead of modeling in frequency domain with a finite order transfer function.

Modeling the lines with an average-friction model effectively reduces the uncertainty between the input to the valve and the output from the actuator. This technique has potential to improve the control performance in pneumatic

tele-operation, when combined with multiple sliding surfaces method established in the last two decades [21], [7]. The multiple sliding surfaces control was developed for a class of non-linear systems that involve a mismatch in the input and output uncertainties. These methods have not been applied for the control of tele-operated pneumatic systems.

In this study, a multiple sliding surface control methodology is proposed to address the transmission line dynamics between the valve and the pneumatic actuator. A line model in time domain is employed to derive multiple control laws arranged in cascade. Unlike existing methods, the formulated controller accounts for the non-linear pressure dynamics in the lines. The benefit of the developed strategy is validated by tele-operated force control experiments that were carried out at a higher frequency and line-length compared to similar studies.

Figure 1 illustrates the key elements of the proposed approach. A virtual input ( $F_V$ ), referred as 'valve force' in this paper, is formulated as a function of pressures at the valve ports ( $P_{V_1}, P_{V_2}$ ). Its relation to the actuator force,  $F_p$ , and the desired mass flow rate towards the actuator,  $\dot{m}_d$ , is characterized by a low-order version of the averaged friction model described by Krichel et al. [10]. The proposed approach consists of two control laws. The first one employs the line model to design a desired virtual input ( $F_{V_d}$ ), which is a reference to the valve force ( $F_V$ ). The second control law ensures the convergence of the valve force to the designed virtual input. In this work, the performance of the proposed method is compared to that of a sliding-mode controller with a standard system model. Force control experiments were conducted on a tele-operated pneumatic actuator, driven by a four-way valve. The comparisons are based on the experimental results with different line lengths at various reference signal frequency.

## III. THE STANDARD SYSTEM MODEL

Pressure dynamics in a pneumatic system has been characterized by combining well-established component models that are briefly summarized in this section for reference. In this standardized approach, shown in Fig. 2, the mass flow rate through the valve is mapped to the actuator pressures. The volumes of the connection tubes are simply added to the corresponding chamber volumes. A typical sliding-mode based (SMC) force controller associated with this model is also described. The performance of this standard SMC was compared to the proposed method that is explained in the following sections.

### A. Chamber Pressure Dynamics

The actuator chambers are typically assumed as isothermal, if the frequency of the pressure variation is low. The volume of the connection tubes ( $V_L$ ) are simply added to the corresponding chamber volumes ( $V_{p_i}$ ). The relation between the mass flow rate through the valve and the chamber pressure is, therefore, formulated as:

$$\dot{P}_{c_i} = \frac{\dot{m}_{v_i} RT - P_{c_i} \dot{V}_{c_i}}{V_{c_i}} \quad (1)$$

where  $i = 1, 2$  and  $V_{c_i} = V_L + V_{p_i}$ .  $R$  represents the thermodynamic constant and  $T$  is the chamber temperature.

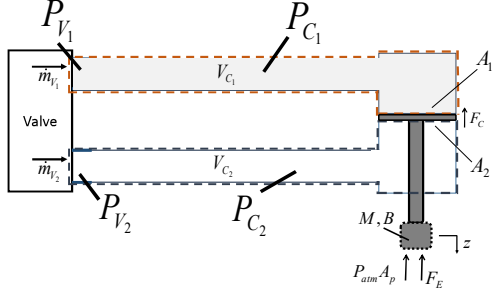


Fig. 2: A standardized pneumatic system model. The pressure along the lines and the actuator chamber is assumed the same. Valve pressures are utilized to calculate the control input for a desired mass flow rate through the valve.

The mass flow through a pneumatic valve port,  $\dot{m}_{v_i}$ , is widely characterized as an isentropic flow through a frictionless orifice, as follows [1]:

$$\dot{m}_{v_i} = C_{(u_v)}\psi(P_{u_i}, P_{d_i}) \quad (2)$$

where  $C_{(u_v)}$  is the net conductance of the valve with a given input command,  $u_v$ , and  $\psi$  is a piecewise function of the upstream pressure,  $P_{u_i}$ , and downstream pressure,  $P_{d_i}$ , across the valve. A detailed formulation of  $\psi$  as well as the relation between the conductance,  $C_{(u_v)}$ , and the valve input command,  $u_v$ , are given in Appendix A. For simplicity, the conductance is referred as the control input, denoted by  $u$ , in this paper.

The assumption of homogeneous pressure and temperature distribution through the system provides a stable model that can be used for actuator pressure estimation in the lack of direct pressure measurement [6]. For the systems that involve long transmission lines, the accuracy of this approach is higher than simply assuming measured valve pressures,  $P_{v_{1,2}}$ , as the actuator chamber pressures,  $P_{c_{1,2}}$  [24].

### B. Piston Dynamics

The magnitude of the force produced by an actuator, referred as actuator force, is given by:

$$F_P = P_{C_1}A_1 - P_{C_2}A_2 \quad (3)$$

The relationship between the external,  $F_E$ , and the actuator force, shown in Fig. 1, is represented by the following equation:

$$F_E = F_P - P_{atm}A_p - M\ddot{z} - B\dot{z} - F_c \frac{|\dot{z}|}{\dot{z}} \quad (4)$$

where  $P_{atm}$  represents the atmospheric pressure,  $A_p$  is the area of the piston rod and  $z$  is the piston displacement. The dynamics of the piston is characterized by an inertia and a damping constant:  $M$  and  $B$  respectively. The external force,  $F_E$ , can be measured by using a force sensor attached to the tip of the piston rod. In our study, possible coulomb friction across the piston,  $F_c$ , is neglected for the actuator being utilized has a graphite piston that produces negligible friction. The relation between the mass flow rates in the system and the dynamics

of the output force can be obtained by substituting (3) to (4), then substituting (1) to the derivative of (4), which yields:

$$(\dot{m}_{v_1} \frac{RTA_1}{V_{c_1}} - \dot{m}_{v_2} \frac{RTA_2}{V_{c_2}}) = \dot{F}_E + G \quad (5)$$

where:

$$G = P_{C_1} \frac{\dot{V}_{c_1} A_1}{V_{c_1}} - P_{C_2} \frac{\dot{V}_{c_2} A_2}{V_{c_2}} + M\ddot{z} + B\dot{z} \quad (6)$$

For a 4-way spool valve that yields an equal net conductance on each port for a given input, the relation in (5) becomes

$$\psi_{T_{(V_{c_1}, V_{c_2})}} u = \dot{F}_E + G \quad (7)$$

where

$$\psi_{T_{(V_{c_1}, V_{c_2})}} = \psi(P_{u_1}, P_{d_1}) \frac{RTA_1}{V_{c_1}} - \psi(P_{u_2}, P_{d_2}) \frac{RTA_2}{V_{c_2}} \quad (8)$$

by substituting (2) to (5).

### C. Standard Sliding-Mode Controller

A typical sliding-mode force control for a pneumatic actuator is implemented by defining a sliding surface based on the error in the output force. Let  $e = F_D - F_E$ , where  $F_D$  is the desired force and the  $F_E$  is the environmental force as described in Fig. 2.b. Choosing a Lyapunov function:

$$L = \frac{1}{2}s^2 \quad (9)$$

on the sliding surface,

$$s = e + \lambda \int edt \quad (10)$$

Stability in the error dynamics, i.e.  $\dot{L} = ss \leq 0$ , is typically ensured by choosing a control input ( $u$ ) that satisfies  $\dot{s} = -ksat(s)$  where:

$$sat(s) = \begin{cases} \frac{s}{\phi}, & \text{if } |s| \leq \phi \\ \frac{s}{|s|}, & \text{if } |s| > \phi \end{cases} \quad (11)$$

with  $\phi$  being a designed boundary thickness for smoothing the input as the sliding surface,  $s$ , converges to the equilibrium [19]. The control input is solved by substituting (7) to the derivative of (10):

$$u = \frac{\dot{F}_D + G + \lambda e + ksat(s)}{\psi_{T_{(V_{c_1}, V_{c_2})}}} \quad (12)$$

### IV. LINE MODELING IN TIME DOMAIN

The tele-operated pneumatic system model developed in this study follows the finite-volume method described in [10]. The transmission line is spatially discretized in its longitudinal axis and the governing equations are implemented on each of the elements with averaged parameter values. Figure 3 presents the elements adopted in our method. In this work, each side of the system is composed of two isothermal control volumes with homogeneous individual pressures and inlet/outlet mass flow across their boundaries. The first volume-element spans the first half of the line towards the valve side. The other half of the line and the actuator chamber combined makes for the

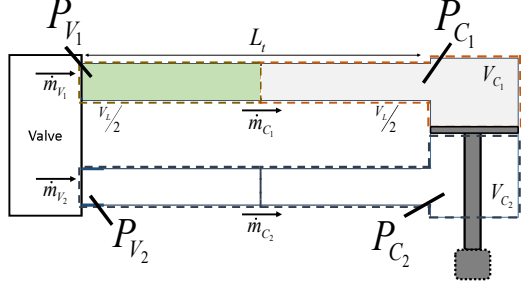


Fig. 3: The schema for the line modeling. The representative pressure for the actuator chamber and valve are shown.

other one. Our model is quasi-static. The following equations are formulated to represent the flow and pressure dynamics of the system:

$$\frac{d\dot{m}_{c_i}}{dt} = (P_{v_i} - P_{c_i}) \frac{A_t}{L_t} - f(\dot{m}_{c_i}, P_{v_i}, P_{c_i}) \dot{m}_{c_i} \quad (13)$$

$$\dot{P}_{c_i} = \frac{\dot{m}_{c_i} RT - P_{c_i} \dot{V}_{c_i}}{V_{c_i}} \quad (14)$$

$$\dot{P}_{v_i} = \frac{(\dot{m}_{v_i} - \dot{m}_{c_i}) RT}{V_L/2} \quad (15)$$

where  $L_t$  is the line length and  $A_t$  is the line cross-section area that defines the volume of the line:  $V_L = A_t L_t$ . Each of the two sides of the pneumatic system, shown in Fig. 3, is denoted by  $i = 1, 2$ . The volume of the actuator chamber is added to the half of the line volume to define the volume associated with  $P_{c_i}$ , i.e.  $V_{c_i} = V_{p_i} + \frac{V_L}{2}$ . The rate of mass flow through the valve,  $\dot{m}_{v_i}$ , is a function of the pressures across the valve and the area of the valve opening given in (2).

This method assumes an averaged tube friction for the whole line that is described by a friction term,  $f$ , multiplied by the mass flow rate through the line,  $\dot{m}_{c_i}$ , in (13). The friction term is approximated by the following function of the mass flow  $\dot{m}_{c_i}$  and the pressures  $P_{v_i}, P_{c_i}$ :

$$f(\dot{m}_{c_i}, P_{v_i}, P_{c_i}) = \frac{32\mu}{D^2} \frac{1}{\rho_i} + 0.158 \frac{\text{Re}_i^{3/4} \mu}{D^2} \frac{1}{\rho_i} \quad (16)$$

where  $\mu$  is the dynamic viscosity of air,  $D$  is the tube diameter,  $\rho_i$  is the density of the air and  $\text{Re}_i$  is the Reynolds number calculated using the mass flow rate,  $\dot{m}_{c_i}$ . This friction formulation is designed to reflect the change in the flow regime from laminar to turbulent with a continuous function. Details on the formulation of the friction term is given in Appendix B. The density,  $\rho_i$ , is calculated by averaging the boundary pressures at the line:

$$\rho_i = \frac{P_{v_i} + P_{c_i}}{2RT} \quad (17)$$

where  $T$  is selected to be the room temperature, assuming isothermal conditions.

The position of the piston, hence the chamber volumes, are calculated and substituted at each time step to obtain the pressure values. Also, the valve pressure is considered to be

available by the use of pressure sensors at the valve ports. Assuming isothermal flow conditions, the state-space model for pressure and flow rate estimation becomes:

$$x = \begin{bmatrix} P_{C_1} V_{C_1} \\ \dot{m}_{C_1} \\ P_{C_2} V_{C_2} \\ \dot{m}_{C_2} \end{bmatrix}, \dot{x} = \begin{bmatrix} \dot{m}_{C_1} RT \\ (P_{V_1} - P_{C_1}) \frac{A_t}{L_t} - f(\dot{m}_{C_1}, P_{V_1}, P_{C_1}) \dot{m}_{C_1} \\ \dot{m}_{C_2} RT \\ (P_{V_2} - P_{C_2}) \frac{A_t}{L_t} - f(\dot{m}_{C_2}, P_{V_2}, P_{C_2}) \dot{m}_{C_2} \end{bmatrix} \quad (18)$$

#### A. Passivity of the Line Model

The tube friction dissipates energy, stabilizing the model estimations. The non-negative friction coefficient in (13) provides a passive mapping from the valve pressure,  $P_{v_i}$ , to the mass flow rate  $\dot{m}_{c_i}$ . Indeed, the stability of the described system for any input valve pressure could be shown when the rate of change in the actuator volume is sufficiently low.

**Theorem 1:** The mapping from the valve pressure,  $P_{v_i}$ , to the mass flow rate,  $\dot{m}_{c_i}$ , described in (18) is passive when the rate of change in the actuator volume is sufficiently low.

**Proof of Theorem 1:** By selecting the mass flow rate,  $\dot{m}_c$ , as the output and the valve pressure as the input, let

$$E = \frac{1}{2} \dot{m}_c^2 + \frac{1}{2} P_c^2 V_c \frac{A_t}{L_t RT} \quad (19)$$

represent the energy developed in the system. The first term in (19) represents the kinetic energy of the flow, whereas the second term refers to the potential energy stored in the actuator chamber. The derivative of  $E$  can be described as follows, substituting (13) and (14):

$$\dot{E} = \frac{A_t}{L_t} \dot{m}_c P_v - f(\dot{m}_c, P_c) \dot{m}_c^2 + \delta_{(\dot{V}_c, P_c)} \quad (20)$$

where  $\delta_{(\dot{V}_c, P_c)} = -\frac{A}{2L_t RT} P_c^2 \dot{V}_c$  is the perturbation due to the variation in the chamber volume. The perturbation is assumed to be bounded, such as  $|\delta_{(\dot{V}_c, P_c)}| < \beta$ , where  $\beta$  is a positive constant. Since the friction function,  $f$ , is always positive for a non-zero mass flow rate; the described mapping is passive when

$$f(\dot{m}_c, P_c) \dot{m}_c^2 > \beta \quad (21)$$

which holds true for sufficiently low rates of change in the chamber volume, i.e. sufficiently low piston velocity. In our study, the targeted force control bandwidth is limited to 2 Hz, which results in a considerably slow piston motion.

This model can be utilized to estimate the chamber pressures ( $P_{C_{1,2}}$ ) and the mass flow rates ( $\dot{m}_{C_{1,2}}$ ) using the measured valve pressures. In addition, the required valve pressure for a desired mass flow rate into the actuator chambers can be calculated.

#### V. CONTROLLER DESIGN

This section introduces the algorithm that ensures a stable force control of tele-operated pneumatic actuators based on the system described in Section IV. In this study, the actuator is assumed to be in contact with an external system with unknown mechanical properties.

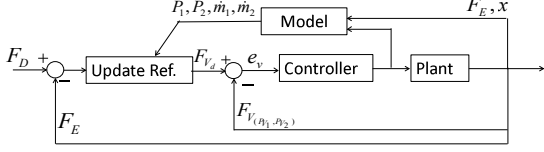


Fig. 4: Block diagram of the proposed cascaded control method

### A. Simplifications

A few simplifications have been made on the line model described in Section IV to simplify the controller implementation and to allow force control with a four-way spool valve. These valves operate on two valve outlets with one electronic input. A discussion on the use of the proposed control idea on different valves is given in Section VIII.

The rate of the pressure change in each actuator chamber can be described by substituting the flow rate shown in (13) to (14):

$$\dot{P}_{c_{1,2}} = (P_{V_{1,2}} - P_{c_{1,2}})h_{1,2} - P_{c_{1,2}}\frac{\dot{V}_{C_{1,2}}}{V_{C_{1,2}}} - \dot{m}_{1,2}\frac{RT}{f(\dot{m}_c, P_c)} \quad (22)$$

where

$$h_{1,2} = \frac{RTA_t}{f_{1,2}V_{C_{1,2}}L_t} \quad (23)$$

The rate of change in the mass flow rate, i.e. the inertia of the air, is neglected and the coefficients  $h_{1,2}$  are unified by averaging the side-specific parameters in each side as follows:

$$\bar{h} = \frac{RTA}{\bar{f}V L_t}, \text{ where } \bar{f} = \frac{f_1 + f_2}{2} \text{ and } \bar{V}_C = \frac{V_{C_1} + V_{C_2}}{2} \quad (24)$$

Substituting (22) to the derivative of (3) and making these simplifications, the rate of change in the piston force,  $F_p$ , given in (3) becomes

$$\dot{F}_p = F_V \bar{h} - F_P \bar{h} - (P_{c_1} \frac{\dot{V}_{C_1}}{V_{C_1}} A_1 - P_{c_2} \frac{\dot{V}_{C_2}}{V_{C_2}} A_2) \quad (25)$$

where

$$F_V = f(P_{v_1}, P_{v_2}) = P_{V_1} A_1 - P_{V_2} A_2 \quad (26)$$

shown in Fig. 1, is defined as valve force in this manuscript.

Averaging the friction coefficients allows for establishing a direct relation between the actuator dynamics and the valve force,  $F_v$ . This simplification would not be necessary if the actuator pressures were individually controlled by separate valves. In our application, the pressures of the four-way spool valve ( $P_{v_1}, P_{v_2}$ ), and the chamber volumes ( $V_{C_1}, V_{C_2}$ ), are measured, whereas the tube friction and chamber pressures are obtained using the original line model described in section IV.

### B. Design of the Controller

The controller is formulated following the general design steps of multiple sliding surface (MSS) control [7]. Consider

the system below, which is obtained based on the simplified line model:

$$\begin{aligned} \dot{F}_E &= F_V \bar{h} - F_P \bar{h} - G + \delta_1(x) \\ \dot{F}_V &= \psi_T(\frac{V_L}{2}, \frac{V_L}{2}) u - \frac{RT(\dot{m}_{c_1} A_1 - \dot{m}_{c_2} A_2)}{V_L/2} + \delta_2(x) \end{aligned} \quad (27)$$

The first equation in the system (27) is obtained by substituting (25) into the derivative of (4). The formulation of  $G$  is given in (6). The second equation is derived by first substituting (15) into the derivative of (26) and then substituting the control input term with the mass flow rates through the valve as shown in (5)-(7).  $\psi_T$  is described in (8). This time  $V_{1,2}$  in (8) is replaced with the first half of the line volume, i.e.  $V_L/2$ .

The perturbation functions  $\delta_1(x)$  and  $\delta_2(x)$  are assumed to be bounded and Lipschitz:  $\delta_1(x) < \beta_1 |x|$  and  $\delta_2(x) < \beta_2 |x|$  with  $\beta_1$  and  $\beta_2$  having positive values.

Two control loops in cascade, one for the desired valve force ( $F_{V_d}$ ) and the other for the desired force output ( $F_d$ ) shown in Fig.4, were formulated. The error in each control loop is defined as below:

$$e_1 = F_D - F_E \quad (28)$$

$$e_2 = F_{v_d} - F_v \quad (29)$$

In the first step, the desired virtual input,  $F_{v_d}$ , is defined as

$$F_{v_d} = F_P + \frac{\dot{F}_D + G}{\bar{h}} + k_{p_1} e_1 + k_{i_1} w_1 \quad (30)$$

where  $w_1 = \int e_1 dt$ ,  $k_{p_1}$  and  $k_{i_1}$  are positive constants. Substituting (28) and (30) into the first relation in (27) gives

$$\dot{e}_1 = -k_{p_1} e_1 - k_{i_1} \int e_1 dt + \bar{h} e_2 + \delta_1 \quad (31)$$

Next step is to select the control input for tracking  $F_{v_d}$ . Let  $u$  be

$$u = \frac{\dot{F}_{v_d} + k_{p_2} e_2 + k_{i_2} w_2 + (\dot{m}_{c_1} A_1 - \dot{m}_{c_2} A_2) \frac{RT}{V_L/2}}{\psi_T(\frac{V_L}{2}, \frac{V_L}{2})} \quad (32)$$

where  $w_2 = \int e_2 dt$  and  $k_{p_2}, k_{i_2}$  are positive constants. Similarly, substituting (29) and (32) into the second relation given in (27) gives

$$\dot{e}_2 = -k_{p_2} e_2 - k_{i_2} \int e_2 dt + \delta_2 \quad (33)$$

**Theorem 2:** The control law, described in (32), satisfies a globally stable force control with regard to the errors in the output force,  $e_1$ , and the virtual input,  $e_2$ .

**Proof of Theorem 2:** The stability of this multi-layer control algorithm can be analyzed by choosing the following Lyapunov candidate:

$$L = \frac{1}{2}(e_1^2 + e_2^2 + (k_{i_1} w_1)^2 + (k_{i_2} w_2)^2) \quad (34)$$

The derivative of the Lyapunov candidate,  $L$ , can be obtained substituting (31) and (33):

$$\dot{L} = -\bar{h} k_{p_1} e_1^2 + \bar{h} e_2 e_1 + \delta_1 e_1 - k_{p_2} e_2^2 + \delta_2 e_2 \quad (35)$$

Using Young's inequality [20],  $ab \leq \frac{\epsilon}{2}a^2 + \frac{1}{2\epsilon}b^2$ , the derivative of  $L$  can be shown as:

$$\dot{L} \leq e_1^2 \bar{h}(-k_{p_1} + \frac{\bar{h}}{2\epsilon_1}) + \delta_1 e_1 + e_2^2 (-k_{p_2} + \frac{\epsilon_1}{2}) + \delta_2 e_2 \quad (36)$$

where

$$e_1 e_2 \leq e_1^2 \frac{\bar{h}^2}{2\epsilon_1} + e_2^2 \frac{\epsilon_1}{2} \quad (37)$$

and  $\epsilon_1$  is a positive constant. Since  $\bar{h}$  is always positive, the errors  $e_1$  and  $e_2$  can be shown to be converging to the following invariant set:

$$\begin{aligned} |e_1| &\geq \left| \frac{\delta_1}{-k_{p_1} + \frac{\bar{h}}{2\epsilon_1}} \right| \frac{1}{\bar{h}} \\ |e_2| &\geq \left| \frac{\delta_2}{-k_{p_2} + \frac{\epsilon_1}{2}} \right| \end{aligned} \quad (38)$$

given that the proportional feedback gains,  $k_{p_1}$  and  $k_{p_2}$ , satisfy:

$$\begin{aligned} k_{p_1} &> \frac{\bar{h}}{2\epsilon_1} \\ k_{p_2} &> \frac{\epsilon_1}{2} \end{aligned} \quad (39)$$

The relation in (39) describes the sufficient condition for stability of the error in the output force. As seen in (31) and (33), the integral gains enable asymptotic error convergence to zero in the steady state, under the condition that the perturbations,  $\delta_1$  and  $\delta_2$ , vary sufficiently slow. Note that the robustness gains in both (31) and (33) act as simple PI control. Instead of constant gain feedback terms, continuous saturation functions with finite boundaries can be designed as shown in [22] if needed. The time derivatives of the position measurement ( $z$ ) and the desired virtual input ( $F_{V_d}$ ) can be numerically approximated. In this study, a first-order filter with a cut-off frequency of 50 Hz was utilized for numerical differentiation.

## VI. EXPERIMENTS

The developed controller was tested on a tele-operated pneumatic actuation set-up with long transmission lines.

### A. Experimental Setup

A double acting cylinder (Airpel E24DU) was connected to a four-way spool valve (Enfield Tech LH-05) via long transmission lines of 4 mm inside diameter. Pressure was measured by analog pressure sensors (SSI Technologies P51 series) at the four locations shown in Fig. 5: at the inlet of each actuator chamber and at each exit port of the spool valve. The pressure measured at the inlet of each actuator chamber was regarded as true pressure in the corresponding chamber and obtained for validating the presented line model. The external force applied to the actuator was measured by a load cell (Omegadyn LC703-50) attached at the tip of the piston rod. The piston was connected to a spring-mass system that represents a contact environment with unknown dynamic parameters, as shown in Fig. 5.b. That system did not include any dampers except an inevitable contact friction in the sliders

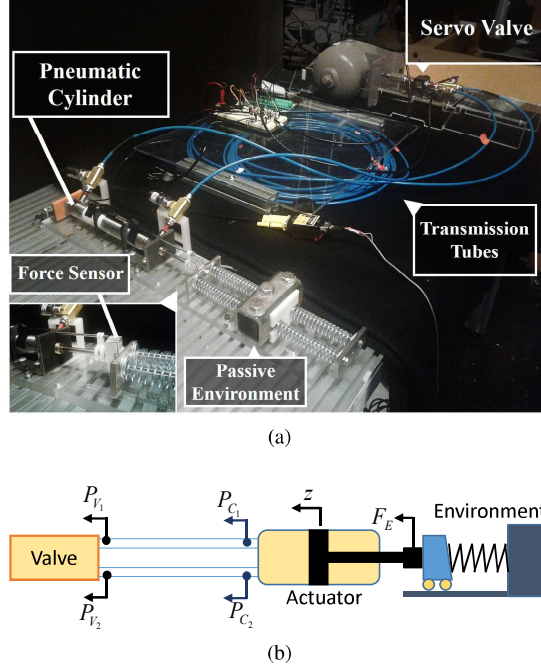


Fig. 5: The experimental setup: a) photo of the test bench b) schema of the components indicating the feedback utilized for force control

that provided a limited damping force. The piston position was measured by using a Honeywell linear potentiometer (model F38000106). The velocity and acceleration of the piston are obtained by numerical differentiation with a first-order filter at 50 Hz. The system was controlled by a platform of Intel i7 @2.80GHz processor with 8.00 GB RAM, where the control algorithm were implemented using Labview. The National Instruments A/D board (NI DAQ-6221) was used for data acquisition.

### B. Procedure

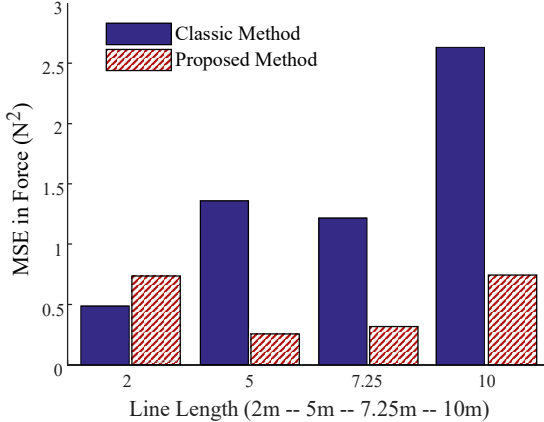
The proposed method was compared to the standard sliding-mode based force controller, described in section III. The performance of each method was tested on four different force reference types: step, 0.5 Hz, 1 Hz, and 2 Hz signals; on four different setups with the following transmission line lengths: 2, 5, 7.25, and 10 meters. The comparison of the accuracy of presented methods was based on the mean of error squares.

The controller gains in each method were tuned to yield an approximate settling time of 0.4s to a step change in the reference force. The values of the gains were kept constant for all reference types on a given transmission line-length.

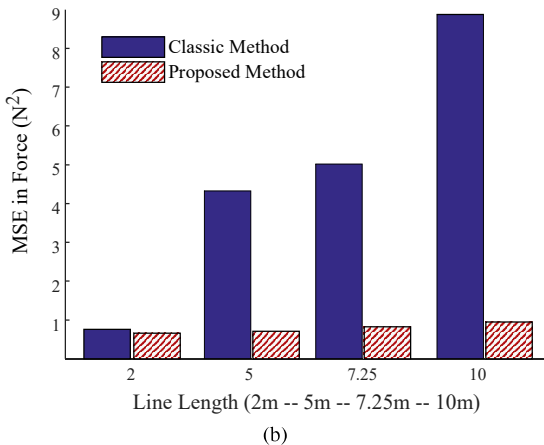
## VII. RESULTS

The proposed method and a standard SMC controller are compared based on the accuracy in force control experiments, as well as actuator pressure estimations. The range of measured piston displacement was less than 4 cm, which makes about a quarter of the stroke length of the actuator.

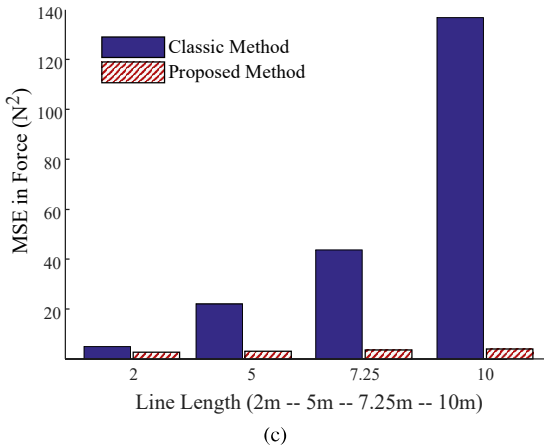
The accuracy in the force control of each method was compared in Fig. 6. The mean of the squared control error,



(a)



(b)

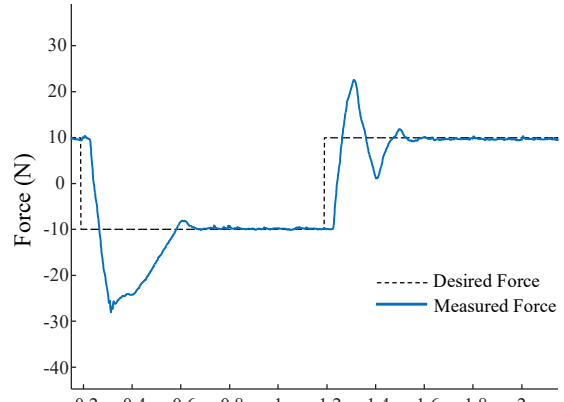


(c)

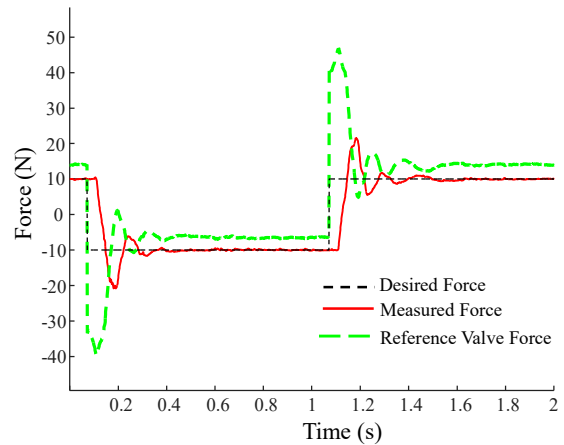
Fig. 6: The accuracy in the force control of both the standard SMC and the proposed method, obtained on setups with different transmission lengths. a) Mean squared control error ( $MSE_F$ ) at 0.5 Hz reference signal b)  $MSE_F$  at 1 Hz reference signal c)  $MSE_F$  at 2 Hz reference signal

$MSE_F$ , was selected as a measure for the assessment of controller accuracy. The diagrams in Fig. 6 refer to 0.5 Hz, 1 Hz and 2 Hz reference signals.

The proposed method achieves the desired force output by tracking the desired virtual input. Figures 7, 8 and 9 show the performance of the analyzed controllers on the tele-operation



(a)



(b)

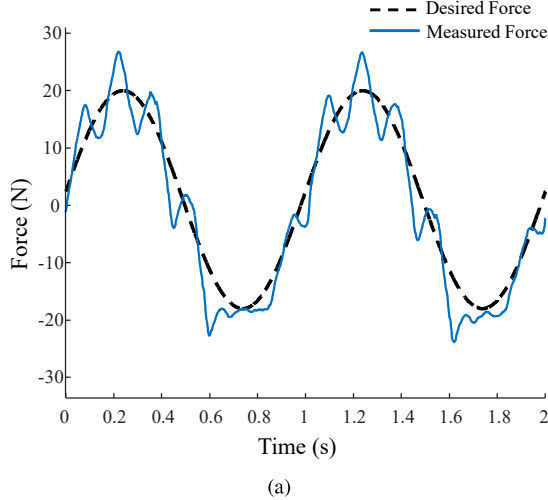
Fig. 7: Output force control performance of the analyzed methods for a step change in the reference force. The transmission length is 10 meters. Performance of a) the standard SMC controller b) the proposed method.

setup with 10 meter long transmission lines. The desired virtual input,  $F_{v_d}$ , generated by the proposed method is added to the corresponding plot in each figure. The accuracy in tracking the desired virtual input was quantified by the mean of the squared tracking error,  $MSE_V$ . The accuracy in the output force control and virtual input tracking for each experiment is given on Table I.

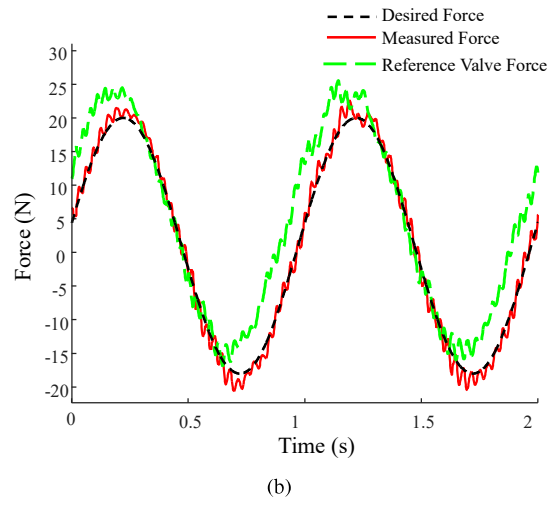
TABLE I: Mean Squared Error in the Output Force Control,  $MSE_F$  ( $N^2$ ), and Virtual Input Tracking,  $MSE_V$  ( $N^2$ )

Line length (m)	0.5Hz $MSE_{F/V}$	1Hz $MSE_{F/V}$	2Hz $MSE_{F/V}$
2	0.74 / 0.82	0.66 / 1.20	2.63 / 8.26
5	0.26 / 1.25	0.70 / 4.78	3.04 / 15.70
7.25	0.32 / 2	0.82 / 7.68	3.51 / 19.35
10	0.74 / 1.35	0.95 / 5.07	4.02 / 12.27

The accuracy in the actuator pressure estimation by the use of the described line model is presented in Fig. 10.a on a 10-meters long tele-operation setup driven at 2 Hz. The mean squared errors in pressure estimations were obtained utilizing the measured actuator chamber pressures. Figure 10.b



(a)



(b)

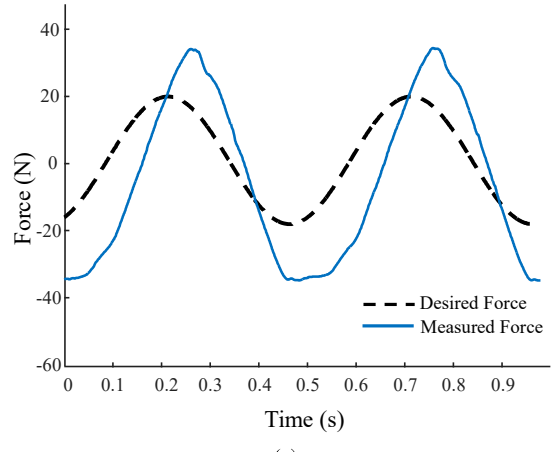
Fig. 8: Output force control performance of the analyzed methods for 1 Hz reference force. The transmission length is 10 meters. Performance of a) the standard SMC controller b) the proposed method.

provides a comparison of the accuracy of each method for various transmission line lengths at 2 Hz reference signal. The estimation errors generally increased with the added length of transmission line.

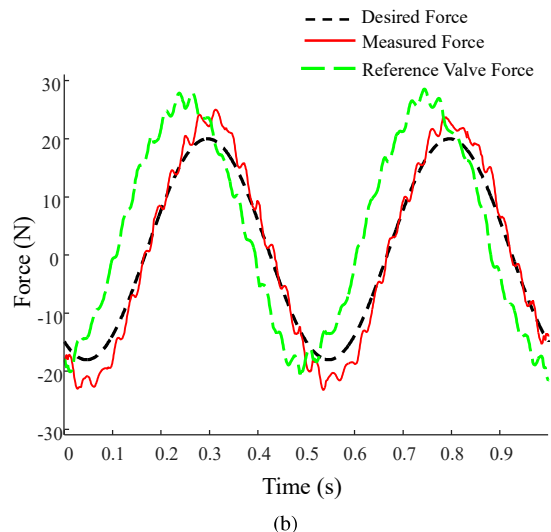
### VIII. DISCUSSION

This study aims to enhance the accuracy in force control of tele-operated pneumatic systems by accounting the dynamics of the transmission lines. Standard pneumatic system models with widely applied sliding-mode controllers neglect the line dynamics previously shown to be very significant on tele-operation [24]. The comparative analysis presented in this work indicates the benefit of an advanced approach that involves the dynamics of the lines.

In general, the contribution of the proposed method becomes more evident as the transmission length and the reference frequency increase. However, the experiments indicate that the described method pays off significantly only if the line length is 5 meters or longer, as shown in Fig. 6. This can be



(a)



(b)

Fig. 9: Output force control performance of the analyzed methods for 2 Hz reference force. The transmission length is 10 meters. Performance of a) the standard SMC controller b) the proposed method.

explained by the influence of the line length on the efficiency of the feedback gain  $k_{p_1}$ . The value of the parameter  $\bar{h}$  increases with a shorter pneumatic tube length. That widens the invariant set to which the error in the output force ( $e_1$ ) converges and decreases the rate of convergence, as seen in (39). At the 2 meter transmission range, the weight of the line volume is small enough to make standard SMC as effective as the proposed cascaded control method. On the other hand, the standard SMC suffers a severe reduction in the force control accuracy beyond the 2-meter range. A similar trend is observed in the influence of operation frequency. Only for the 2-meter transmission range at 0.5 Hz reference, the accuracy of standard SMC is higher than that of the proposed method. In that configuration, the performance of both controllers were affected by the uncertainty of the valve calibration that is more significant at small valve opening ranges. A small volume setup with a low actuation frequency generally results in a low operation range, resulting in calibration-related mismatches.

The desired virtual input,  $F_{V_d}$ , represents the target force

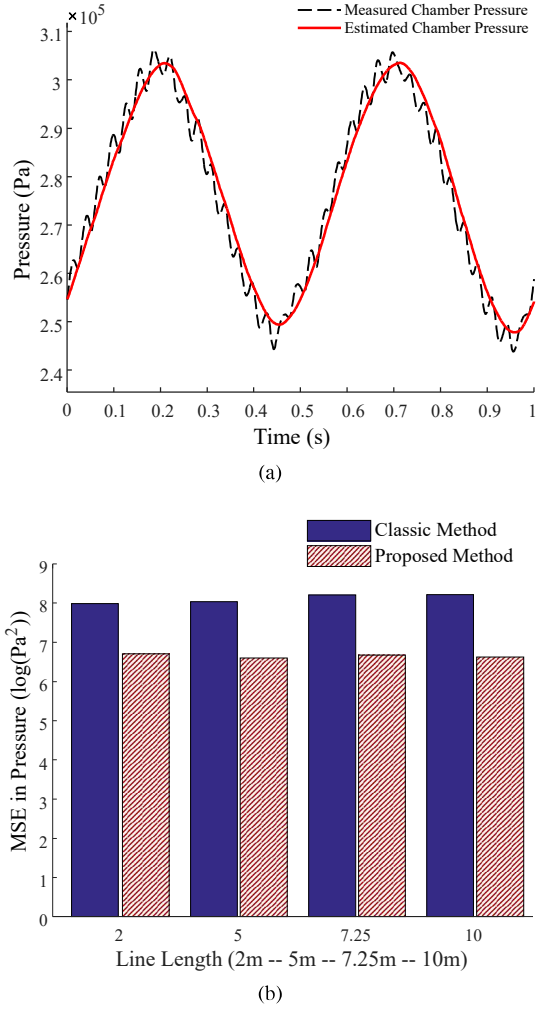


Fig. 10: Measured and estimated actuator pressures for the setup with 10 meters long transmission at 2 Hz force reference. a) Estimation performance of the described line model. b) The mean squared error (MSE) in actuator chamber pressure estimation. The standard model is compared to the proposed line model on various transmission lengths with 2 Hz reference signal. Note that the Y axis is in logarithmic scale in this graph.

profile at the inlet of the transmission lines. As shown in Figs. 7 to 9, that the reference valve force signal appears to be slightly shifted to the left in time, and upward in magnitude. This emergent negative phase shift is the reason for the improvement in force control. The proposed method compensates for the dynamic delay due to the lines, matching the valve force,  $F_V$ , with the desired virtual input,  $F_{V_d}$ . The upward shift in magnitude compensates for the static difference between the actuator force,  $F_P$ , and the environmental force,  $F_E$ , which is  $P_{atm}A_p$  in (4). That static difference can be seen in Fig. 7.b more clearly.

The developed multiple sliding surface controller has gain limitations attributable to the compressible flow dynamics in the transmission lines. The control method employs force and position feedback from the actuator that is separated from the point of control input, the valve. The inner dynamics between

the source of feedback and the point of input leads to coupled instability, inducing chattering in the system pressures and force output. Note that the actuator is coupled with a spring-mass system which is the most challenging environment type for contact stability [8]. The resonance in the system pressures throughout the lines and the proximity to the external pressure sources (reservoir and ambient) result in greater oscillations in the valve pressures. This leads to comparatively elevated error magnitudes for the inner control loop, as indicated in Table I. Omitted in this manuscript, a reduction in the oscillations, and therefore in  $MSE_V$ , was observed by selecting less aggressive control gains for the inner loop at the expense of a slight increase in the output force control errors,  $MSE_F$ . Despite the vulnerability to coupled instability, the proposed method provides a superior accuracy compared to the standard alternative that employs a low-order model. Moreover, it maintains the accuracy in the output across the selected transmission ranges.

Dividing the transmission line into two segments, by following the finite control-volume method described in [10], improved the pressure estimation drastically, as seen in Fig. 10.b. The error magnitudes are presented in the logarithmic scale due to an order of magnitude difference in between. More line segments could provide a higher accuracy in open-loop pressure and flow rate estimations. In this work, the number of line segments, hence the order of the model, is designed to match the number of sliding surfaces defined in (28) and (29), which enabled the proof of stability given in section V. With the limited number of segments and a conservative friction calculation, the presented model filtered out the chatters in the actuator pressures, as seen in Fig. 10.a.

This study demonstrates the efficacy of the proposed method in the accuracy of force control of tele-operated pneumatic actuators, particularly at high frequencies (1-2 Hz). The method can be used to implement impedance control on haptic applications such as rehabilitation in magnetic resonance imaging (MRI) rooms. It does not require pressure measurements at the actuator and maintains its efficiency in the 5-10 meters transmission range, which is the typical transmission length in magnetic resonance imaging (MRI) compatible robotic devices [28], [11]. Yu et al. has compared hydraulic and pneumatic actuation with regard to their use in tele-operation. They reported that the moderate bandwidth of the pneumatic actuation is a major advantage of pneumatics over hydraulics [29]. Within the same bandwidth, the proposed method is effective in maintaining the control accuracy as the reference signal frequency rise. Another interesting application would be pneumatically actuated exoskeletons or humanoids. Transmission lines are needed for separating the system components to achieve a desirable weight distribution. In such applications, the connection tubes are relatively short, but they are smaller in diameter [18]. Therefore, they can potentially affect the flow dynamics.

The proposed control method involved simplifications to enable its use with four-way spool valves by a single input. The inner closed-loop was designed to make the flow-controlled spool valve act as a pressure-controlled servo. The introduced idea can be utilized for independent pressure control by the

use of separate valves without the need for the simplifications presented in the Section V.a. Such hardware implementations have been suggested for force and stiffness control in the previous research [30], [17], [22].

## IX. CONCLUSION

Compressible flow through pneumatic transmission lines complicate the control of tele-operated pneumatic actuators and reduce the accuracy of conventional control methods. In this paper, a multiple sliding surface controller that utilizes transmission line modeling was proposed and experimentally validated. The performance of the described method was compared to a sliding-mode controller with a standardized system model. The experiments showed a significant improvement in the accuracy in force control for systems with 5-10 meters long transmission lines between the actuator and valves.

The introduced controller demonstrated the importance of accounting for the line dynamics and the efficiency of the cascaded control strategy for the force control of pneumatically driven tele-operated systems. The proposed method has a potential to improve the quality of physical interaction between humans and tele-operated pneumatic systems, which is crucial for MRI-compatible therapy devices or pneumatically actuated humanoids. This study provided an experimental proof of the efficiency of the developed control method on tele-operation tasks, leaving the potential applications as future work.

## REFERENCES

- [1] P. Beater. *Pneumatic drives*. Springer, 2007.
- [2] D. B. Comber, E. J. Barth, and R. J. Webster. Design and Control of an Magnetic Resonance Compatible Precision Pneumatic Active Cannula Robot. *Journal of Medical Devices*, 8(1):011003, Dec. 2013.
- [3] A. Elmasry and M. Liermann. Passive pneumatic teleoperation system. In *ASME/BATH 2013 Symposium on Fluid Power and Motion Control*, pages V001T01A040–V001T01A040. American Society of Mechanical Engineers, 2013.
- [4] E. Franco, M. Rea, W. Gedroyc, and M. Ristic. Control of a master-slave pneumatic system for teleoperated needle insertion in mri. *IEEE/ASME Transactions on Mechatronics*, 21(5):2595–2600, 2016.
- [5] E. Franco and M. Ristic. Adaptive control of a master-slave system for teleoperated needle insertion under mri-guidance. In *Control and Automation (MED), 2015 23th Mediterranean Conference on*, pages 61–67. IEEE, 2015.
- [6] N. Gulati and E. Barth. A Globally Stable, Load-Independent Pressure Observer for the Servo Control of Pneumatic Actuators. *IEEE/ASME Transactions on Mechatronics*, 14(3):295–306, June 2009.
- [7] J. Hedrick and P. Yip. Multiple sliding surface control: theory and application. *Journal of dynamic systems, measurement, and control*, 122(4):586–593, 2000.
- [8] N. Hogan and S. P. Buerger. Impedance and interaction control, 2005.
- [9] Iso 6358:1989 pneumatic fluid power - components using compressible fluids - determination of flow-rate characteristics, 1989.
- [10] S. V. Krichel and O. Sawodny. Non-linear friction modelling and simulation of long pneumatic transmission lines. *Mathematical and Computer Modelling of Dynamical Systems*, 20(1):23–44, Jan. 2014.
- [11] L. Lacey, M. A. B. D., V. J., and U. J. Design of mri-compatible hemiparesis rehabilitation device. *Journal of Medical Devices*, 8(2), 2014.
- [12] J. Li, K. Kawashima, T. Fujita, and T. Kagawa. Control design of a pneumatic cylinder with distributed model of pipelines. *Precision Engineering*, 37(4):880–887, Oct. 2013.
- [13] G. Pegman, B. Luk, K. Liu, A. Collie, D. Cooke, and S. Chen. Tele-operated climbing and mobile service robots for remote inspection and maintenance in nuclear industry. *Industrial Robot: An International Journal*, 33(3):194–204, 2006.
- [14] G. Pratt and M. Williamson. Series elastic actuators. In *Intelligent Robots and Systems 95. 'Human Robot Interaction and Cooperative Robots', Proceedings. 1995 IEEE/RSJ International Conference on*, volume 1, pages 399–406 vol.1, Aug 1995.
- [15] E. Richer and Y. Hurmuzlu. A high performance pneumatic force actuator system: Part i-nonlineair mathematical model. *Journal of dynamic systems, measurement, and control*, 122(3):416–425, 2000.
- [16] E. Richer and Y. Hurmuzlu. A high performance pneumatic force actuator system: Part ii-nonlineair controller design. *Journal of dynamic systems, measurement, and control*, 122(3):426–434, 2000.
- [17] X. Shen and M. Goldfarb. Simultaneous force and stiffness control of a pneumatic actuator. *Journal of dynamic systems, measurement, and control*, 129(4):425–434, 2007.
- [18] K. Shorter, J. Xia, E. Hsiao-Wecksler, W. Durfee, and G. Kogler. Technologies for powered ankle-foot orthotic systems: Possibilities and challenges. *Mechatronics, IEEE/ASME Transactions on*, 18(1):337–347, Feb 2013.
- [19] J.-J. E. Slotine, W. Li, et al. *Applied nonlinear control*, volume 199. Prentice-Hall Englewood Cliffs, NJ, 1991.
- [20] B. Song, A. Howell, and K. Hedrick. Dynamic surface control design for a class of nonlinear systems. In *Decision and Control, 2001. Proceedings of the 40th IEEE Conference on*, volume 3, pages 2797–2802. IEEE, 2001.
- [21] D. Swaroop, J. K. Hedrick, P. P. Yip, and J. C. Gerdes. Dynamic surface control for a class of nonlinear systems. *IEEE transactions on automatic control*, 45(10):1893–1899, 2000.
- [22] B. Taheri, D. Case, and E. Richer. Force and stiffness backstepping-sliding mode controller for pneumatic cylinders. *Mechatronics, IEEE/ASME Transactions on*, 19(6):1799–1809, 2014.
- [23] E. Todorov, C. Hu, A. Simpkins, and J. Movellan. Identification and control of a pneumatic robot. In *Biomedical Robotics and Biomechatronics (BioRob), 2010 3rd IEEE RAS and EMBS International Conference on*, pages 373–380. IEEE, 2010.
- [24] M. Turkseven and J. Ueda. An asymptotically stable pressure observer based on load and displacement sensing for pneumatic actuators with long transmission lines. *IEEE/ASME Transactions on Mechatronics*, 2016.
- [25] M. Turkseven and J. Ueda. Observer based impedance control of a pneumatic system with long transmission lines. In *Robotics and Automation (ICRA), 2016 IEEE International Conference on*, pages 1160–1165. IEEE, 2016.
- [26] J. Watton. The dynamic performance of an electrohydraulic servo-valve/motor system with transmission line effects. *Journal of dynamic systems, measurement, and control*, 109(1):14–18, 1987.
- [27] P. Wongputorn, D. Hullender, R. Woods, and J. King. Application of matlab functions for time domain simulation of systems with lines with fluid transients. *Journal of fluids engineering*, 127(1):177–182, 2005.
- [28] B. Yang, U.-X. Tan, A. McMillan, R. Gullapalli, and J. Desai. Design and control of a 1-dof mri-compatible pneumatically actuated robot with long transmission lines. *Mechatronics, IEEE/ASME Transactions on*, 16(6):1040–1048, Dec 2011.
- [29] N. Yu, C. Hollnagel, A. Blickenstorfer, S. Kollias, and R. Riener. fmri-compatible robotic interfaces with fluidic actuation. *Robotics: Science and Systems IV, Zurich, Switzerland, June*, pages 25–28, 2008.
- [30] Y. Zhu and E. J. Barth. Impedance control of a pneumatic actuator for contact tasks. In *Robotics and Automation, 2005. ICRA 2005. Proceedings of the 2005 IEEE International Conference on*, pages 987–992. IEEE, 2005.

## X. APPENDIX

### A. The Valve Model

The function  $\psi$  is defined as follows [1]:

$$\psi(P_u, P_d) = \begin{cases} \frac{|A_v|}{A_v} P_u \rho_0 \sqrt{\frac{T_0}{T}} & \text{if } \frac{P_d}{P_u} \geq b \\ \frac{|A_v|}{A_v} P_u \rho_0 \sqrt{\frac{T_0}{T}} \sqrt{1 - (\frac{P_d}{1-b})^2} & \text{if otherwise} \end{cases} \quad (40)$$

where  $T$  is the stagnation temperature of the gas,  $\rho_0$  and  $T_0$  are density and temperature of air at reference conditions respectively [9],  $b$  is the critical ratio of the pressures that determines whether the flow is choked or unchoked, and  $R$  is the ideal gas constant.  $C_{u_v}$  is the sonic conductance of the

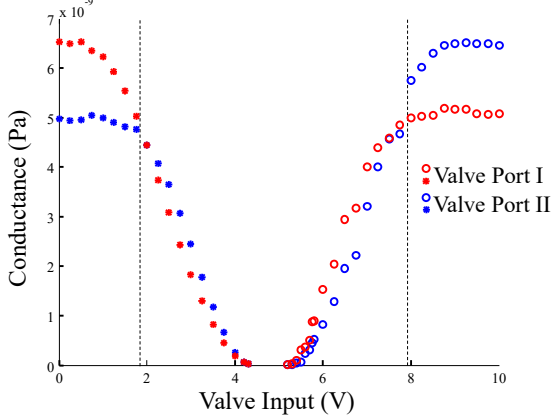


Fig. 11: The valve calibration obtained by fixed chamber flow tests [9]

valve that is characterized by a low order polynomial of the valve input,  $u_v$ ; hence, the orifice area,  $A_v$ . The inlet and exit pressures of the valve are assigned accordingly:

$$\begin{aligned} P_u &= P_{res}, P_d = P_{act} && \text{if } A_v \geq 0 \\ P_u &= P_{act}, P_d = P_{atm} && \text{if otherwise} \end{aligned}$$

where  $P_{res}$  is the reservoir pressure,  $P_{act}$  is the chamber pressure and  $P_{atm}$  is the ambient pressure. In this research, the dynamics of the spool of a valve is neglected as the valve's bandwidth is significantly higher than the bandwidth of pneumatic dynamics.

The relation between the sonic conductance and the valve input has been empirically obtained through the calibration routines explained in [9]. The measured conductance of each orifice size in the valve is shown in Fig. 11. The values of the net conductance of the ports are assumed to be equal except if the valve command is between 0-2 V, or 8-10 v. For those valve command intervals the control input,  $u$ , and the desired valve command,  $u_v$  are solved simultaneously.

### B. Friction in the Pipe Flow

The resistance force,  $F_f$ , due to the friction along a transmission tube of length  $L_t$  is described as [10]:

$$F_f = \lambda \frac{L_t A_t}{D} \rho \frac{v^2}{2} \quad (41)$$

where  $\lambda$  is the Darcy-Weisbach friction coefficient and  $v$  is the velocity of the fluid, which is assumed to be homogeneous across the cross-section of the tube. The Darcy-Weisbach friction coefficient has been accurately characterized for fully-developed flow regimes: laminar and turbulent, yielding the following piecewise function for the resultant force [1]:

$$F_f = \begin{cases} 32 \frac{\mu}{D^2} L_t \dot{m}, & \text{if } Re \leq 2300 \\ 0.158 Re^{3/4} \frac{\mu}{D^2} L_t \dot{m}, & \text{if } Re \geq 4600 \end{cases} \quad (42)$$

where Reynolds number is represented by  $Re = \rho u \frac{D}{\mu}$ , and  $\dot{m} = \rho u A_t$  is the mass flow rate. The flow is considered to be in a transitional phase when  $2300 \leq Re \leq 4600$ , where the flow is unsteady. In this study, a global and continuous

representation is formulated to prevent chattering due to the regime fluctuations in the flow:

$$\hat{F}_f = \left( \frac{32\mu}{D^2} \frac{1}{\rho} + 0.158 \frac{Re^{3/4}\mu}{D^2} \frac{1}{\rho} \right) \dot{m} \quad (43)$$

This simple approximation over-estimates the friction loss, especially in the transitional flow regime, which contributes to the stability margin of the line model as shown in (21).

**Melih Turkseven** received the B.S. degree from Bogazici University, Istanbul, Turkey, in 2010, and the PhD degree from Georgia Institute of Technology, Atlanta, USA, in 2016, both in mechanical engineering. He is currently working as a post-doctoral research associate at Rensselaer Polytechnic Institute in the area of haptics. His current research interests include mechanical design, control of dynamical systems, bio-inspired robotics and medical robotics.

**Jun Ueda** received the B.S., M.S., and Ph.D. degrees from Kyoto University, Kyoto, Japan, in 1994, 1996, and 2002, respectively, all in mechanical engineering. From 1996 to 2000, he was a Research Engineer with the Advanced Technology Research and Development Center, Mitsubishi Electric Corporation, Hyogo, Japan. From 2002 to 2008, he was an Assistant Professor in the Graduate School of Information Science, Nara Institute of Science and Technology, Nara, Japan. From 2005 to 2008, he was a Visiting Scholar and Lecturer in the Department of Mechanical Engineering, Massachusetts Institute of Technology, Cambridge. Since 2008, he has been with the George W. Woodruff School of Mechanical Engineering, Georgia Institute of Technology, as an Assistant Professor. His current research interests include vibration control, robust control, mechanical design, and biologically inspired robotics. Dr. Ueda is a co-recipient of the 2009 IEEE Robotics and Automation Society Early Academic Career Award.